Measuring internal forces in single-stranded DNA: Application to a DNA force clamp

Megan C. Engel,[*,†,‡] Flavio Romano,[¶] Ard. A. Louis,[‡] and Jonathan P. K. Doye[§]

†*School of Engineering and Applied Sciences, Harvard University, 29 Oxford Street, Cambridge MA, 02138, USA*

‡*Rudolf Peierls Centre for Theoretical Physics, University of Oxford, 1 Keble Road, Oxford, OX1 3NP, UK*

¶*Dipartimento di Scienze Molecolari e Nanosistemi, Universitá Ca Foscari di Venezia, Via Torino 155, 30172, Venezia Mestre, Italy*

§*Department of Chemistry, University of Oxford, South Parks Road, Oxford, OX1 3QZ, UK*

E-mail: mcengel@seas.harvard.edu

Abstract

We present a new method for calculating internal forces in DNA structures using coarse-grained models and demonstrate its utility with the oxDNA model. The instantaneous forces on individual nucleotides are explored and related to model potentials, and using our framework, internal forces are calculated for two simple DNA systems and for a recently-published nanoscopic force clamp. Our results highlight some pitfalls associated with conventional methods for estimating internal forces, which are based on elastic polymer models, and emphasize the importance of carefully considering secondary structure and ionic conditions when modelling the elastic behavior of single-stranded DNA. Beyond its relevance to the DNA nanotechnological community, we expect our approach to be broadly applicable to calculations of internal force in a va-

riety of structures – from DNA to protein – and across other coarse-grained simulation models.

1 Introduction

The communication of force is central to cellular function. Force propagation through DNA features in transcription and translation, as the double helix is unzipped by molecular machines;[1,2] in the compression of ∼metres of DNA into a ∼6 µm-diameter nucleus;[1] and even in gene expression, which is is modulated by the mechanical state of the nucleus.[3] Force plays a role in manifold other biological mechanisms, as well: mechanosensitive ion channels open in response to specific tension in cellular membranes;[4,5] the catalytic activity of enzymes can be altered by the application of force;[4] and the cytoskeleton and extracellular matrix are tensegrity networks that propagate forces within, between, and among cells.[6] Force and torque are also central to the operation of molecular machines, from transport molecules like kinesin to ATP synthase, the universal cellular energy production factory.[7] Because of their critical role in diverse processes, from embryogenesis[8] to immune response[9,10] and tumor metastasis,[11] probing forces at the molecular level is a key scientific aim.

The advent of DNA nanotechnology[12,13] has enabled the fabrication of DNA-based nanoscale devices capable of sensing[14–16] and exerting[2,16–18] forces in the biologically relevant regime of 0-20 pN.[19] DNA force sensors have already been profitably applied to study integrin proteins that connect cells to extracellular filaments;[20] the forces involved in nucleosome association;[21] and DNA repair proteins.[14] Force-generating DNA devices have been used to investigate the binding of transcription factors under tension[2,17] and to mimic the function of molecular motors in transporting cargo.[18] These devices exploit the mechano-elastic properties of DNA in its single- and double-stranded forms. Some sense forces using the known rupture forces of double-stranded DNA (dsDNA) in unzipping or shearing geometries.[22] Others use the unfolding thermodynamics of DNA hairpins:[23–27] when hairpins unfold in response to an applied

load, it is inferred that the force exceeds $F_{1/2}$, the force at which a hairpin has a 50% chance of being unfolded at equilibrium. In computing $F_{1/2}$, elastic polymer models are typically employed to calculate the free energy of stretching single-stranded DNA (ssDNA). Polymer models are also invoked to calibrate nanodevices that capitalize on the *entropic spring* behavior of ssDNA, which resists any decrease in configurational entropy: circumscribing the end-to-end distance of ssDNA by even a few nm leads to forces in the pN range.[28,29] Sensors use the end-to-end distances of ssDNA to report forces,[19,21] and other devices exert predefined forces on targets by constraining the end-to-end distance of ssDNA.[2,17,30,31]

Many nanotechnological applications beyond force sensors and probes require knowledge of the mechano-elastic properties of ssDNA: some nanostructures are designed to experience constant stress,[32] which is mediated by ssDNA in the DNA origami kites and tensegrity prisms of Liedl et al.[33], for example. The DNA helix bundles in these structures were able to assemble against a force of $\sim$14 pN applied by ssDNA linkers.[33] DNA wireframe arcitectures, such as polyhedra and buckyballs,[34,35] feature flexible ssDNA strands as vertices that link stiff double-stranded regions to achieve designed shapes. ssDNA springs have furthermore been used to introduce flexibility into DNA origami crank-slider joints;[36] to act as hinges in nanocages designed for drug delivery;[37] and as components of nanotubes capable of the controlled release of gold nanoparticles.[38] Finally, many computational models utilized to refine and design DNA nanostructures employ polymer models of ssDNA,[39,40] rendering the importance of accurate mechanical models of DNA far-reaching.

To determine the forces exerted on or applied by ssDNA in biological and nanotechnological contexts, two general routes have been employed: experimental calibration and simplified polymer models.[15] In the former case, single-molecule force spectroscopy (SMFS), for example via magnetic tweezers, is used to characterize the force response of the tension sensor in question.[19,25] SMFS experiments are prone to instrumental artefacts, however, including convolution of tension probe with the instrument response function and the fact that bond rupture forces depend on loading rates[41,42] used during calibration. These issues complicate

the interpretation of forces and lead to uncertainties of at least ∼a few pN.[19,25]

Alternatively, because ssDNA has been widely described by simplified polymer models – typically the worm-like chain (WLC)[43] or the extensible freely-jointed chain (exFJC)[44] model – the majority of DNA tension probes are calibrated by applying such models with previously-measured parameters.

One example of a DNA tension probe calibrated using simplified polymer models is the recently-proposed DNA origami force clamp of Nickels et al.[17], shown in Figure 1. Force is applied to a molecule of interest bound to the centre of a ssDNA spring suspended between rigid origami blocks; the magnitude of this force can be tuned by adjusting the spring's length. In practice, this is achieved by altering the internal origami staple sequences slightly to thread portions of ssDNA 'reservoirs' on either end of the origami into or out of the central gap. As we will detail below, potential problems with common calibration procedures like the one employed by Nickels et al.[17] include the fact that it is not clear how to map ssDNA straightforwardly to existing polymer models, as well as the existence of secondary structures in ssDNA which they do not account for.

Given the challenge of calculating ssDNA internal forces precisely and the relevance of doing so to manifold biological and nanotechnological applications, simulations have a clear role in complementing and refining experiments. However, an explicit procedure for calculating these forces in coarse-grained simulations has not been delineated elsewhere. Here, we present a novel method for calculating internal forces in coarse-grained simulations. We then use this framework to analyse the nanoscopic force clamp of Nickels et al.[17], which allows us to highlight crucial pitfalls associated with using continuum polymer models to calibrate internal forces in ssDNA.

To achieve our end of providing accurate internal force estimates in a DNA nanostructure, a computational model of DNA is needed that is detailed enough to capture DNA mechanics well, but sufficiently coarse-grained that it can be simulated on long enough time scales to (i) sample all relevant ssDNA secondary structure and (ii) achieve a converged

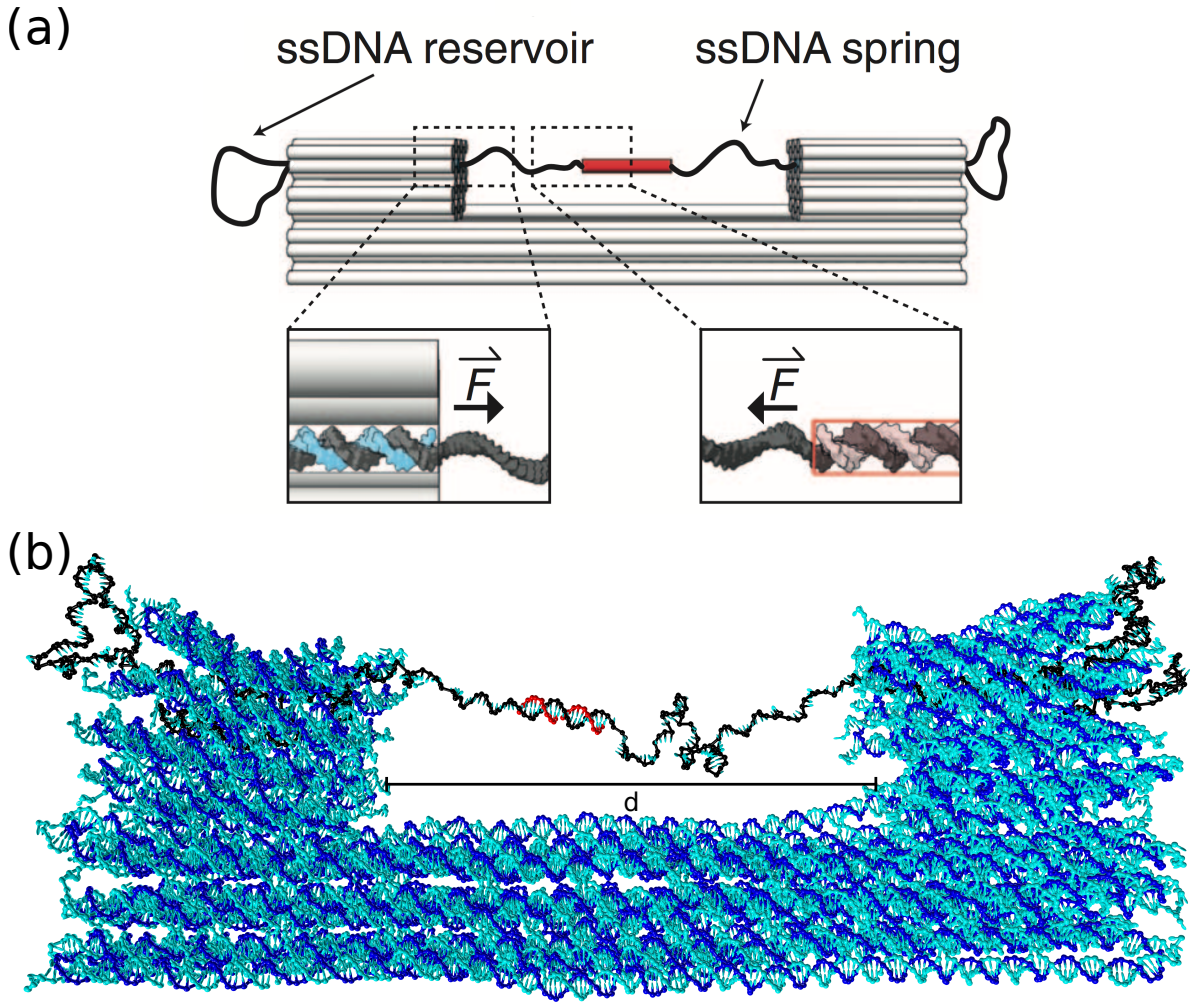

Figure 1: Illustrations of the force clamp designed by Nickels et al.[17]. (a) a schematic and (b) an oxDNA representation of the force clamp. A length of ssDNA to which the system of interest is bound (red) is suspended across the gap in the DNA origami frame. Its length, and hence the tension, can be adjusted by altering the origami design such that material is transferred between the ssDNA 'reservoirs' (black) and the central gap. (a) is adapted with permission from Nickels et al.[17]. The distance across the gap d is designed to be 42.84 nm.

average over instantaneous forces that may have large variance. Here, we use oxDNA,[45–47] a single-nucleotide-level coarse grained DNA model that has enjoyed extensive validation at multiple levels of description. Basic DNA biophysical properties, including structure, persistence length,[45–47] torsional modulus,[48,49] and the force-extension curves of single- and double-stranded DNA[46] are well-captured by oxDNA, which also successfully modelled force-induced dsDNA overstretching.[50] Additionally, oxDNA has successfully described large DNA origami designs both structurally – capturing the opening angles of DNA origami hinges[51,52] and the full 3D structure of a cryo-EM characterized origami[53] – and mechanically, reproducing experimental origami force unfolding behavior.[54] Finally, oxDNA has repeatedly been shown to capture the thermodynamics of DNA hybridization and hairpin formation reactions well.[45–47] Since these are the crucial processes relevant to ssDNA secondary structure formation, we are confident that oxDNA is capable of sampling secondary structures realistically; indeed, previous studies have validated this ability explicitly through deriving ssDNA secondary-structure-dependent quantities that matched closely with experimental values.[50,55] By combining oxDNA molecular dynamics (MD) simulations of the aforementioned force clamp with our method for calculating internal forces, we demonstrate the importance of simulation-aided force calibration for DNA nanotechnological applications.

2 Methods

2.1 oxDNA Simulations

The oxDNA model has been presented and characterized in detail elsewhere.[45–47] oxDNA is a nucleotide-level coarse-grained model featuring three interaction sites per nucleotide, corresponding to backbone, stacking, and hydrogen-bonding interactions. The model was parametrized in a "top-down" fashion, using experimental data on DNA structure, thermodynamics, and mechanics. Interactions between nucleotides are mediated by pairwise potential functions designed to capture relevant physics, and the current version of the model,

oxDNA2, incorporates electrostatics according to Debye-Hückel theory in addition to the previously included terms for excluded volume, backbone connectivity, hydrogen bonding, base stacking, cross stacking (i.e. stacking between bases on opposite duplex strands), and coaxial stacking (i.e. stacking between contiguous bases on different strands, as across a nick). While the model can capture the effects of salt concentration, temperature, and sequence-dependence, it cannot represent the detailed interactions of DNA with solvent ions, though this shortcoming is not expected to affect the current work significantly. One additional, important caveat is that oxDNA currently cannot represent non-canonical base pairing, which could potentially affect its ability to model ssDNA secondary structures accurately. We do not believe this limitation to be consequential to our results, however, as detailed further below.

We performed MD simulations with oxDNA, using the velocity Verlet algorithm to integrate Newton's equations of motion with an integration time step of 15.2 fs. Solvent in oxDNA is implicit, and we simulated our systems in the canonical NVT ensemble. Coupling between the system of interest and a heat bath was imitated using an Andersen-like thermostat,[56,57] where velocities were redrawn from a Maxwell-Boltzmann distribution every 1.55 ps. The particle translational diffusion coefficient was set to 2.5, or $6.0 \times 10^{-7}\,\mathrm{m^2\,s^{-1}}$ – which is about $\sim$2 orders of magnitude faster than in experiment[58] – to accelerate diffusive dynamics and improve sampling. This change in the effective diffusion coefficient does not affect the equilibrium properties that we are calculating in this paper.[59] For the simulations of the full origami structure shown in Figure 1, GPUs were used; otherwise, simulations were performed on CPU.

Before collecting data for analysis, all systems simulated in this work were equilibrated until the potential energy reached a stable value. Simulations were performed at 21 °C and at varying monovalent salt concentrations, as detailed below. Complete simulation parameters used can be found in Table S1 in the Supporting Information.

2.2 Calculating forces

In order to calculate the internal tension in a polymer using a coarse-grained simulator such as oxDNA, some average over the pairwise particle forces must be taken. Because nucleotides can interact with more than just their nearest neighbors, the correct way to find the average force at any point in the chain is to draw a 'topological interface' between two nucleotides in the DNA structure (for example, the red dashed lines in Figure 2) and sum forces exerted by all nucleotides *topologically downstream* of the interface on all nucleotides *topologically upstream* of the interface. On average and at equilibrium, the force directed topologically upstream $\rightarrow$ downstream will be equal in magnitude to the force directed topologically downstream $\rightarrow$ upstream, and will be the net tension in the chain. In this and subsequent sections, we refer to the force calculated in one topological direction (upstream $\rightarrow$ downstream or vice versa) as the 'one-sided' force. In principle, given sufficient sampling, the one-sided force will be the same regardless of where in the DNA structure one draws the interface. Note that the sum of oppositely-directed one-sided forces at any interface should give zero at equilibrium for a polymer at rest.

Figure 2(a) illustrates these concepts schematically with a single strand featuring a small hairpin. For simplicity, consider only the backbone interactions – modelled in oxDNA by a finitely extensible nonlinear elastic (FENE) potential and indicated by straight lines – and hydrogen bonding interactions – indicated by the pink curved lines. A naive approach to calculating the tension in the strand connecting nucleotides 3 and 4, for instance, is to find the total one-sided force on nucleotide 3 from 'upstream': the sum of the forces exerted on it by nucleotides 4 and 5, $\mathbf{F}_3^+$ in Fig. 2(a). This general strategy yields inconsistent forces across the polymer, with very large forces in regions of secondary structure, apparent in Figure 4(b). Because we expect a constant one-sided tension throughout the polymer chain at equilibrium, it is clear that a different approach is needed. In the case of the example of Figure 2(a), the force exerted by nucleotide 6 on nucleotide 2 by virtue of their hydrogen bond must also be included, to correctly counterbalance the complex force propagation dynamics in the

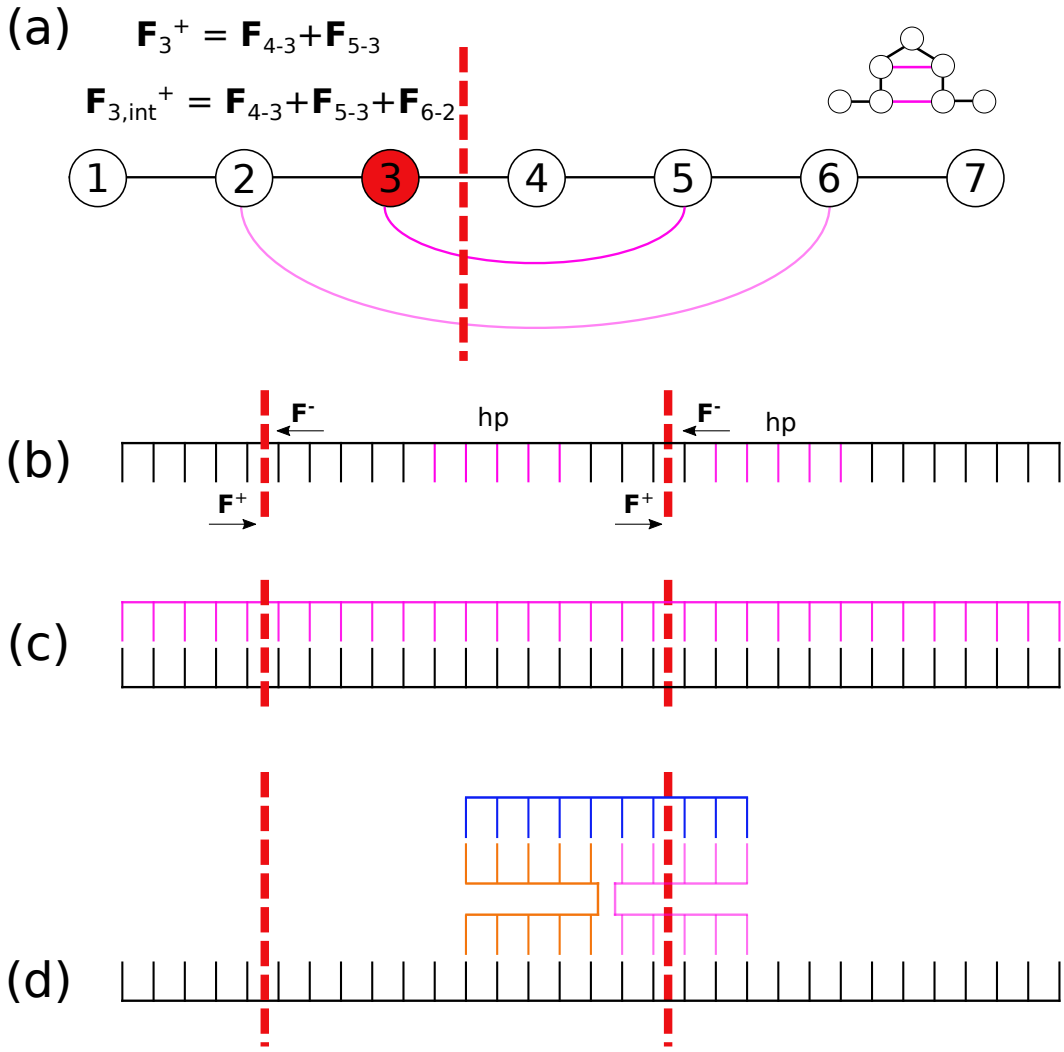

Figure 2: (a) A schematic of our approach for measuring the internal tension in DNA structures. For simplicity, consider nucleotides linked only through a backbone potential (straight lines) and hydrogen-bonded base pairs (pink, curved lines). The ssDNA depicted contains a 2 nucleotide hairpin stem with a 1 nucleotide loop, 'unrolled' from the configuration shown in the upper right. Calculating the one-sided force on nucleotide 3 from topologically upstream yields $\mathbf{F}_3^+ = \mathbf{F}_{4-3} + \mathbf{F}_{5-3}$. The net force thus computed neglects an important counterbalancing term and yields too-large forces (Fig. 4(b)) near to and within the hairpin. Instead, the total force exerted on *all* nucleotides to the left of a virtual interface (red dashed line) by *all* nucleotides to the right of that interface should be computed: $\mathbf{F}_{3,\mathrm{int}}^+ = \mathbf{F}_{4-3} + \mathbf{F}_{5-3} + \mathbf{F}_{6-2}$. The approach is illustrated for 3 representative DNA structures: (b) a single strand containing a hairpin (pink, indicated with 'hp'); (c) a double strand; (d) a single strand with a Holliday junction. Red dashed lines are interfaces across which the net force is calculated.

hairpin; this yields $\mathbf{F}^{+}_{3,\mathrm{int}}$ in Fig. 2(a). The example discussed in reference to Figure 4 below confirms that this is the correct approach where one desires to compute the spatially-constant net internal tension across a polymer chain. Figure 2(b)–(d) illustrate example topological interfaces for a single strand with a hairpin, a double strand, and a single strand containing a Holliday junction, respectively. Here and in subsequent sections, we use the notational convention that $\mathbf{F_i}^{+}$ ($\mathbf{F_i}^{-}$) indicates the one-sided force directed topologically downstream $\rightarrow$ upstream (topologically upstream $\rightarrow$ downstream) at a given nucleotide or interface location i in the polymer. Note that the topological direction must be distinguished from the *physical* direction of the force. We indicate components of the force along particular physical axes using subscripts; for example, $F^{+}_{i,x}$ is the x-component of the topologically downstream $\rightarrow$ upstream one-sided force on nucleotide i (for calculations involving the naive method) or across interface i (for calculations involving the topological interface method).

In the sections that follow, we find the internal strand tension for test cases of a poly-T strand, ssDNA with a hairpin, and the nanoscopic force clamp of Nickels et al.[17] that was discussed above.

3 Test systems

3.1 poly-T ssDNA

Consider first a simple test case of a single 160-nucleotide (nt) poly-T strand whose ends are trapped in harmonic potentials, shown in Figure 3(a). Constraining the endpoints should give rise to a nonzero tension in the strand. In this case, a naive attempt to compute this tension by summing the forces on a given nucleotide exerted by all other nucleotides topologically upstream of it yields similar values all along the chain: Figure 3(b) displays in black the component of the one-sided force along the axis of constraint, here the y-axis, labelled '$F^{+}_{i,y}$', and equal to 3.84 pN when averaged over all 160 nucleotides. The average one-sided force component along each of the axes perpendicular to the axis of constraint is

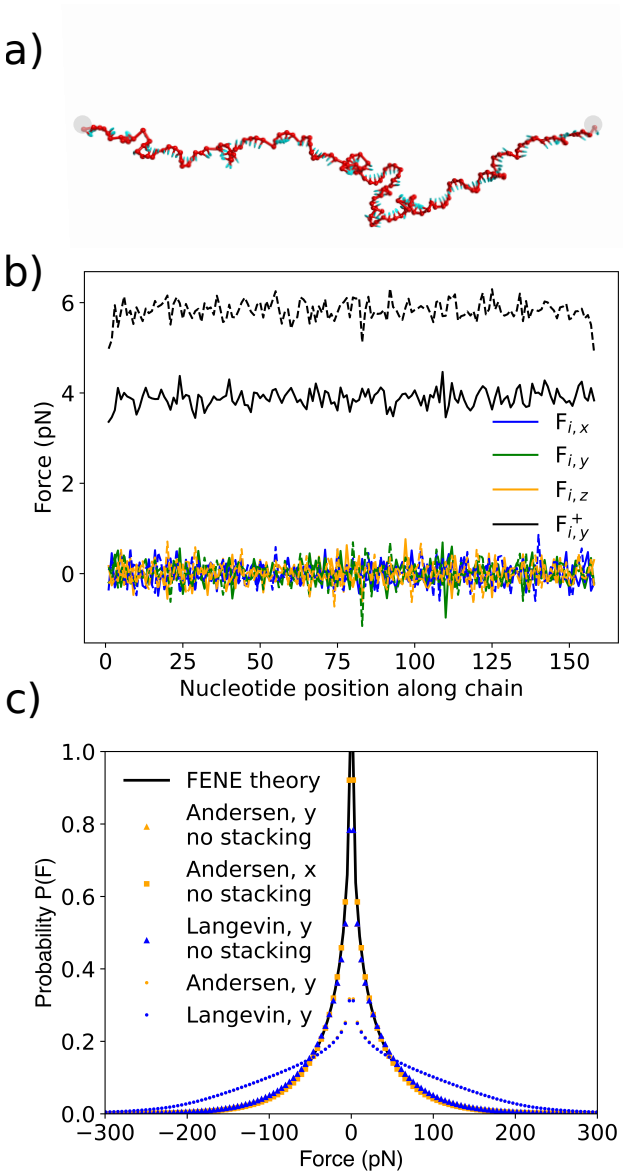

Figure 3: (a) oxDNA representation of the 160-nt poly-T system, with end nucleotides subjected to harmonic traps (grey spheres). (b) Average forces in the single-stranded DNA. Colored lines depict the total force exerted on each nucleotide by all others, in all three directions. The black curves, labelled '$F^{+}_{i,y}$', represent the 'one-sided' force on nucleotide i along the direction of constraint, calculated using the naive method discussed above: the net force exerted on a nucleotide by all nucleotides topologically upstream of it. The force that is obtained when base-stacking interactions are turned off is given by the dashed black curve. (c) Probability distributions for the force averaged over all nucleotides in the strand of (a), both with the standard oxDNA model (circles) and with stacking interactions suppressed (triangles and squares), using two different thermostats. Note that the results for the Andersen thermostat with no stacking (yellow triangles) are almost completely overlapped by the results for the Langevin thermostat with no stacking (blue triangles). Forces are net forces exerted on each nucleotide by all others, and are shown along the direction of constraint y and along an orthogonal axis x. The theoretical prediction if force is only mediated by the FENE potential is given by the black line.

$\sim$0 pN. Additionally, the *net* force on each nucleotide ($\mathbf{F_i}^{\text{net}} = \mathbf{F_i}^{+} + \mathbf{F_i}^{-}$) averages to $\sim$0 pN, as it should for a chain in equilibrium that is experiencing no net acceleration. Simulations were repeated with the base stacking interaction turned off; the resulting average force of $\sim$5.79 pN, shown by the dashed black line in Figure 3(b), is higher than with stacking turned on. This is physically reasonable: a chain that is stacked has a longer Kuhn length than one that is unstacked, and has fewer conformations available to it; thus, its internal tension is lower.

We can compare this force to the prediction of the exFJC model:

$$\langle x \rangle = L_c \left(\coth\left(\frac{F\ell}{k_B T}\right) - \frac{k_B T}{F\ell} \right) \left(1 + \frac{F}{S}\right), \tag{1}$$

where F and $\langle x \rangle$ are the force and average extension, respectively; S is the stretch modulus; $L_c = N\ell$ is the contour length of the chain; and $k_B T$ is the usual thermal energy. Under our simulation conditions, and using the frequently-cited parameters of Smith et al.[28]: Kuhn length $\ell = 1.5$ nm, contour length L_c =160 nt $\times$ 0.56 nm, and elastic modulus $S = 800$ pN, the exFJC model predicts an entropic tension in the chain of $\sim$4.4 pN. That this is higher than the simulated result reflects that the experimental fits of Smith et al.[28] are averaging over secondary structure, which is not present in the poly-T.

We note that the effective force shown in Fig. 3(b) is an average, and that instantaneous forces can be much larger. To analyse this further we report in Fig. 3(c) the distribution of forces experienced by an individual nucleotide along the chain (averaged over all 160 nucleotides in the chain) for two directions: along the axis of constraint (y) and orthogonal to this axis (x), and for two different thermostats: Langevin (described on pages 1-2 in the Supporting Information) and Andersen-like. Results for the two axes are in good agreement, as are the results for the two thermostats, thus confirming that the distributions are not artefacts of a particular thermostat choice. The first noteworthy feature is that the distributions are very broad, with instantaneous forces over 100 pN in magnitude being common; therefore, averages must be computed over large amounts of data to derive sensible average

force estimates (the values in Figure 3(b) represent averages over 3.8×10^{10} MD timesteps, or ∼0.6 ms.[1]). Secondly, they are non-Gaussian. Finally, force distributions corresponding to the full simulations (circles) are broader than those with stacking turned off (triangles and squares). In both cases, the considerable magnitude of the forces and the shapes of the distributions can be rationalized by looking in detail at the underlying oxDNA potentials.

In a single strand of poly-T DNA, the two main routes for internucleotide force transfer are backbone interactions, mediated by the FENE potential, and base stacking. The force probability distribution expected if interactions are due solely to the FENE potential can be derived; see pages 2-4 of the Supporting Information for details. The resulting $P(F)$ is plotted in black in Fig. 3(c), and matches well the data from simulations with stacking interactions suppressed.

The form of the stacking potential in oxDNA can be used to understand why force distributions are broadened by stacking interactions. A rough estimate of representative forces at equilibrium due to each of the FENE and stacking potentials is given by the derivatives of these potentials (considering only the radial term of the stacking potential for simplicity) evaluated at the thermal energy that the system is expected to possess in equilibrium according to equipartition, $k_BT/2$; see pages 4-6 of the Supporting Information for details. Using oxDNA parameters, representative radially-directed forces are are $F_{FENE}^{thermal} \sim 89\,\mathrm{pN}$ and $F_{stack}^{thermal} \sim 193\,\mathrm{pN}$, which, after taking into account that only one component of the force is plotted in Fig. 3(c), match the distribution widths well.

3.2 ssDNA with hairpin

Consider now a more complex arrangement: a 160-nt strand that is poly-T save for a hairpin with a 10-bp stem and a 4-T loop near to the 5' end of the strand; see Figure 4(a). Applying

[1]In oxDNA, simulation time units can be converted to physical units based on simulation energy and length scales; this conversion yields 3.03×10^{-12}s per time unit. The simulations performed in this work used 200 MD steps per time unit, corresponding to ∼15 fs per MD step. However, comparison of coarse-grained MD timescales to actual physical timescales must be done cautiously, due to the fact that coarse-graining reduces timescale separations between different processes.[60] This can be done in general by comparing the physical (experimental) and simulation timescales for a relevant process.[61]

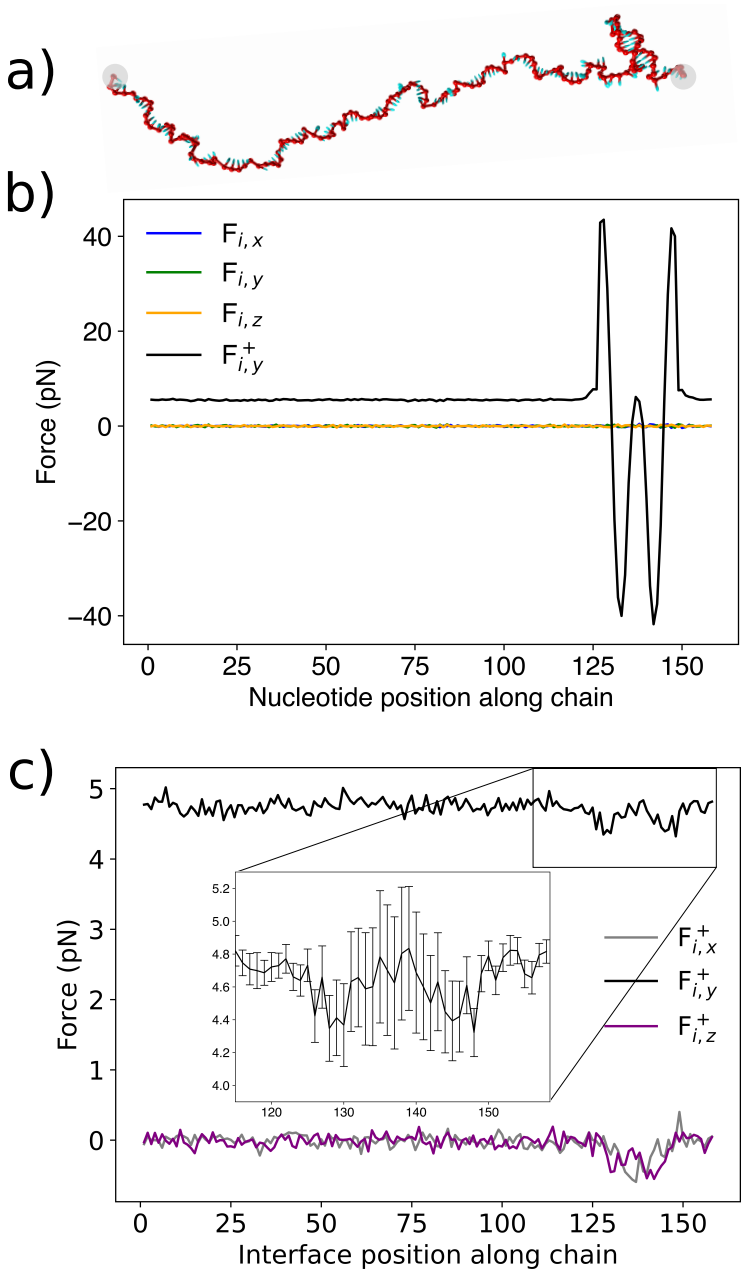

Figure 4: (a) An oxDNA configuration for a strand identical to that of Fig. 2(a), but with a hairpin with a 10 bp-stem and a 4-T loop near to the right-hand end. (b) The net forces exerted on each nucleotide by all other nucleotides in each dimension (yellow, green, blue), along with the one-sided force – the net force exerted on each nucleotide by all nucleotides topologically upstream of it – along the axis of constraint (black, $F^+_{i,y}$). The presence of the hairpin makes the force propagation along the strand more complex. (c) One-sided forces computed instead using the topological interface method described in the text. Here, interface position i indicates an interface drawn immediately topologically upstream of nucleotide i, as in Figure 2. The inset shows the region containing the 10-base pair hairpin in more detail. Error bars are standard errors of the mean from 64 identical parallel simulations; these tend to be larger near to the hairpin because of the larger magnitude of forces in this region. As expected, the tension along the constraint direction ($F^+_{i,y}$) is non-zero.

the method of section 2.2 to calculate internal tension no longer works, as revealed by Figure 4(b). The net force exerted on each nucleotide is still 0 pN on average, as it should be. However, while one expects the average one-sided force on each nucleotide along the direction of constraint to be approximately constant and equal to the entropic tension in the strand, this is not the case in the vicinity of the hairpin. It is apparent that, when analyzing tension in a DNA chain where secondary structure is involved, it is no longer sufficient to simply calculate the forces exerted on each nucleotide by all nucleotides topologically 'upstream' or 'downstream' of it, as force propagation in that case is mediated by a more complex network of interactions – including hydrogen bonding and cross-stacking – that communicate tension through the chain in a non-trivial manner. That the deviations in $F_{i,y}^{+}$ forces in the hairpin region are so large partly reflects the features of the oxDNA potential, which in turn are capturing the physical frustration inherent to DNA interactions. In particular, even in cases where there is no net tension in the strand, bases in double-stranded regions like the hairpin stem cannot simultaneously minimize hydrogen-bonding, stacking, backbone, and cross-stacking potentials. This is evidenced by the fact that, for example, a stacked single strand has a tighter helix than dsDNA[62] and that base-paired nucleotides have a small propeller twist.[63] Because they are displaced from the minima of one of more of these potentials, the average individual inter-nucleotide forces in the vicinity of the hairpin can be large; hence, when only a subset of the forces across a topological interface are taken into account, there will be large deviations from the true force being transmitted through the chain.

The approach described above in *Methods*, however – adding *all* forces directed topologically upstream $\rightarrow$ downstream across a given interface – recovers the expected results: see Fig. 4(c). In this case, the tension averaged across all nucleotides along the axis of constraint is ~ 4.8 pN (higher than in the poly-T case previously considered because the hairpin has shortened the effective contour length), and the force behaves reasonably in the vicinity of the hairpin, though errors in that region are larger due to the greater magnitude of pairwise

nucleotide forces.

3.3 Nanoscopic force clamp

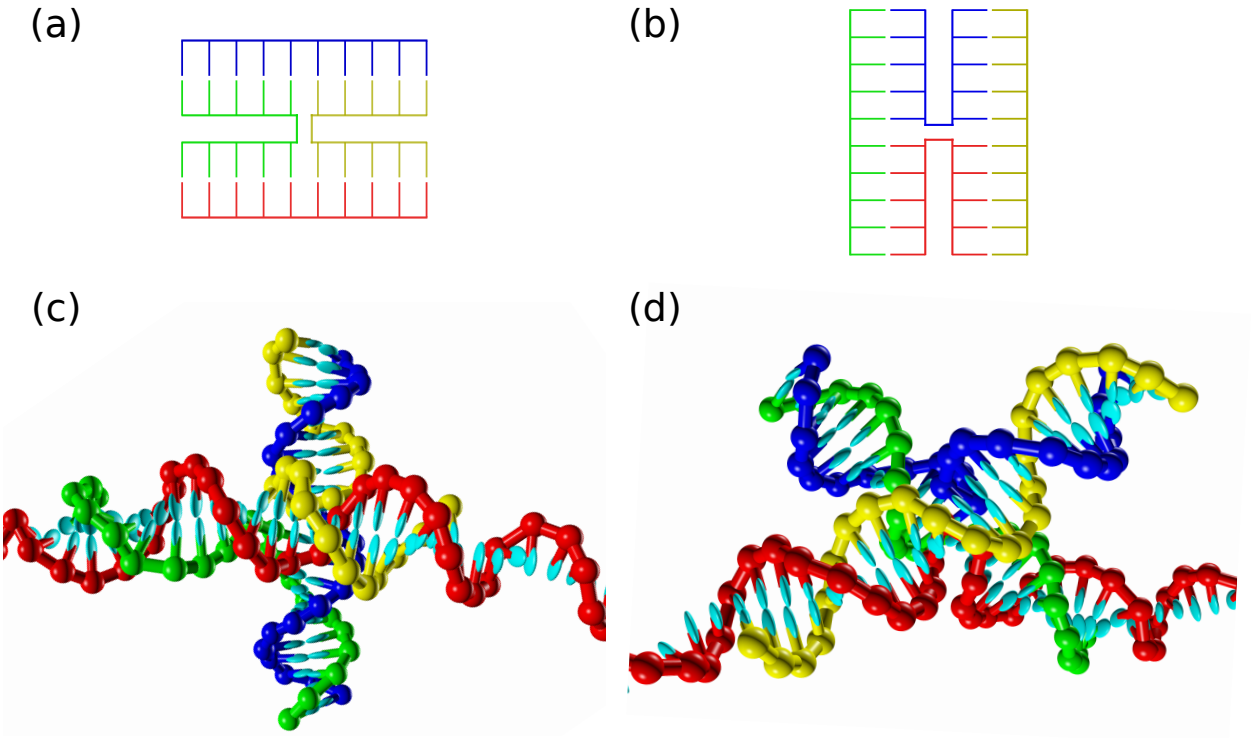

Figure 5: (a), (b) Schematics and (c), (d) oxDNA configurations for the two possible coaxially-stacked isomers of the Holliday junction. In IsoII (left) the coaxial stacking occurs between the green and yellow strands, whereas in IsoI (right) the coaxial stacking occurs between the blue and red strands. The red strand is part of a longer ssDNA section (see Fig. 6 for a zoomed-out view) along which a force is exerted. This force adds a thermodynamic bias that favors IsoII.

With some improved understanding of the mechanisms of force propagation in oxDNA simulations and the appropriate methods for calculating internal forces in hand, we turn our attention to the more interesting case of the nanoscopic force clamp of Nickels et al. [17], described in the *Introduction*.

Their design solves many of the issues with traditional force spectroscopy apparatus like atomic force microscopes and laser optical tweezers, and is a powerful addition to the toolbox used to investigate mechanical processes in the cell. In particular, because it is instrument-

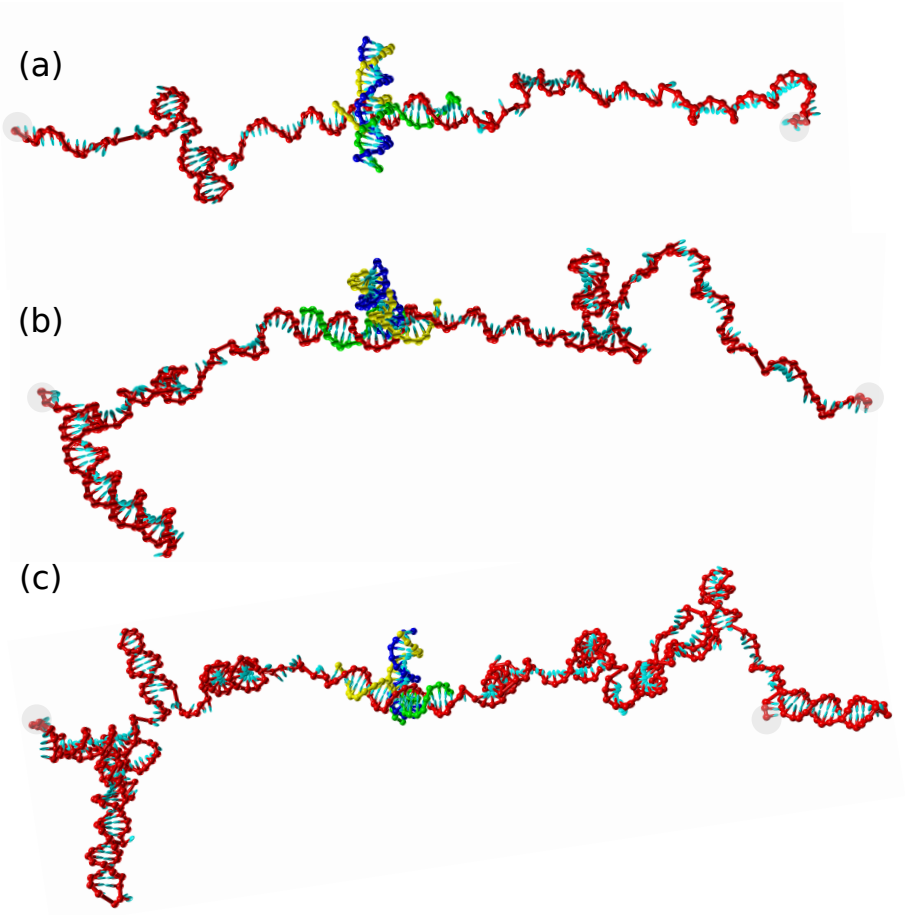

Figure 6: oxDNA configurations of the ssDNA segment that spans the gap of the force clamp and that has a Holliday junction near to its centre. The designed forces for the three systems are (a) 4.0 pN, (b) 2.5 pN, and (c) 1.2 pN. The total number of nucleotides in the red strand in each of these cases is 162, 228 and 424, respectively. The propensity of this sequence to form secondary structure is clear, and becomes more prevalent at lower forces, as expected.

free, many of the artefacts that plague single molecule force spectroscopy (SMFS) experiments – for example, convolution with long linker handles[64] – are not a concern. The design furthermore enables large numbers of single-molecule experiments to be performed in parallel due to its highly scalable nature. Traditional experimental SMFS methods are by contrast necessarily serial, leading to poorer statistics. Finally, the requirement of attachment to microscope apparatus precludes conventional SMFS experiments from being performed *in vivo*, while nanoscopic force clamps circumvent this limitation. Nickels et al. used their force clamp to study the Holliday junction[65] and the tension-dependent binding of the TATA protein.[17] The precise forces exerted on the systems of interest were calculated as follows:

- the origami was assumed to be completely rigid;
- the ssDNA was replaced with an exFJC polymer with end-to-end distance given by the designed gap size minus the average extension of the molecule of interest;
- parameters for Kuhn length, contour length, and elastic modulus derived from previous experiments were plugged into the exFJC force-extension equation and combined with the end-to-end distance estimates to yield forces.

Three potential problems with this procedure, elements of which many DNA tension probe studies share,[2,20,23,24,26,27,33] bear consideration. Firstly, while dsDNA is well-described by the WLC,[66–68] ssDNA behavior is difficult to capture with simplified polymer models. Authors have used both WLC and exFJC to fit ssDNA in different regimes, dependent on ionic conditions and force.[69,70]

The rigidity of ssDNA increases with decreasing ionic concentrations due to electrostatic repulsion, so the WLC model may offer a better description of ssDNA than the exFJC in low-salt conditions.[69] Both models, however, neglect excluded volume and stacking interactions between ssDNA bases. Difficulties inherent in mapping ssDNA to a WLC or exFJC emerge when comparing elastic parameters obtained from experiments performed at zero force (where bases are free to stack) and force-pulling experiments (featuring higher forces

at which stacking is less favorable) that feature a clear stacked → unstacked transition.[70,71] A dependence of fit parameter on experimental regime is widespread in the literature,[28,70,72,73] but interestingly this has not been extensively acknowledged.

A second issue with force probe calibration using polymer models is the existence of sequence-dependent secondary structures in ssDNA, which reduce the effective contour length of ssDNA and elevate internal forces. One of the most widely-used sets of ssDNA elastic parameters is that derived by Smith et al.[28], who fitted force-extension curves of λ-DNA to the exFJC. These parameters represent an average over λ-DNA secondary structure and are thus not transferrable to different ssDNA sequences.

Finally, assumptions about the rigidity of the origami portion of the force clamp could introduce errors into the force estimates. DNA origami, of course, have some degree of flexibility,[74] but the elastic mechanical properties have only been characterized for a limited number of rod-like origami.[75,76]

As mentioned, Nickels et al.[17] demonstrate the operation of their nanoscopic force clamp by studying the four-way Holliday junction[65](HJ), a fundamental component of DNA origami designs. HJs are comprised of 4 strands hydrogen-bonded to each other and arranged in an 'X' shape. In the presence of salt, the strands coaxially stack (i.e. bases belonging to two separate strands stack with one another) to adopt one of two possible isomeric conformations, illustrated in Figure 5. In Fig. 5(a) and (c), the green and yellow strands are coaxially stacked, and the blue and red strands are regularly stacked such that they are straight; the reverse is true in Fig. 5(b) and (d). External force applied to the HJ can tune the population ratio between the isomers. If force is applied to both ends of the red stand in Fig. 5, for example, the dwell time in the configuration pictured in Fig. 5(a) will increase. Nickels et al.[17] refer to this more energetically favorable isomeric state as 'IsoII', and the less favorable isomer, in which the tension-bearing strand is bent, as 'IsoI', drawing their nomenclature from the low (IsoI) and high (IsoII) FRET states for a particular geometry of donor/acceptor dyes on the chosen HJ sequence, following Hohng et al.[65]. We adopt here

the same convention.

Nickels et al.[17] constructed three versions of the origami force clamp to illustrate the force-dependence of the population ratios of IsoI and IsoII. The authors named these designs the 4.0 pN, 2.5 pN, and 1.2 pN versions, referring to the predicted forces the ssDNA springs would exert on the molecule of interest in each clamp. These predicted force calculations were performed according to the exFJC model, Eq. 1, using the Kuhn length and stretch modulus parameters reported by Smith et al.[28]; the number of nucleotides spanning the central gap in each design (160, 4.0 pN; 226, 2.5 pN; 422, 1.2 pN) minus the 22 nucleotides corresponding to the HJ region; a contour length per base pair of 0.63 nm, derived from crystallographic experiments;[77] and the designed central gap width of 42.84 nm – labelled d in Fig. 1 – minus the average end-to-end extension of the HJ as the polymer end-to-end distance, $\langle x \rangle$. Notably, the magnesium ion concentration at which the force clamp experiments were performed – 100 mM [Mg^{2+}] – represents much higher electrostatic screening than the salt concentration used in the experiments of Smith et al.[28], 150 mM [Na^{+}], because Mg^{2+} has been estimated to have an effect that is 20-100× stronger than Na^{+},[70,78] depending on the property that is being studied. High ionic strengths are often used in DNA origami experiments to facilitate origami assembly.

3.3.1 Simulation strategy

For our purposes of determining the internal forces in the single-stranded section of the origami force clamp, it was not necessary to simulate the full origami structure in the force-measurement simulations. Instead, we simulated only the ssDNA strand in the central gap of the force clamp and represented the constraints placed on the single strand by the origami with harmonic traps (where the stiffness and separation of the traps were extracted from simulations of the full origami), thus vastly improving the statistics we were able to collect in our available simulation time. To achieve this, we first performed an MD simulation of the origami force clamp with no connecting single strand, and monitored the end-to-end

distance r between scaffold nucleotides on either end of the clamp; the results are shown in Figure S2. The resulting distribution was fit to a Gaussian form:

$$P(r) = Ae^{-\frac{(r-\langle r \rangle)^2}{2\sigma^2}} \tag{2}$$

to extract the mean $\langle r \rangle = 42.77\,\text{nm}$ and variance $\sigma_r^2 = 0.50\,\text{nm}^2$. Note that $\langle r \rangle$ is approximately equal to the value used by Nickels et al.[17] based on simple geometrical arguments: 42.84 nm. The values for $\langle r \rangle$ and $\langle \sigma_r^2 \rangle$ can be reproduced by two 3-dimensional harmonic traps of stiffness $k = 16.32\,\text{pN/nm}$ and trap separation $d = 42.76\,\text{nm}$ acting on the end nucleotides of the tension-bearing single strand (the approach used to obtain these values is detailed on pages 6-7 of the Supporting Information). We note that by only simulating the force-bearing strand, we are ignoring potential interactions between this section and the rest of the origami (aside from these 3D harmonic traps on its ends). These interactions will be predominantly due to the excluded volume, but given the design (e.g. the clearance above bridging section) we don't expect their effects to be significant.

We performed MD simulations on the ssDNA + HJ system, with end nucleotides harmonically trapped, for the three different force designs of Nickels et al.[17]. Including the two trapped endpoint nucleotides, the main ssDNA strands comprised 162-nt, 228-nt, and 424-nt for the 4.0 pN, 2.5 pN, and 1.2 pN designs, respectively. As is evident in Figure 6, secondary structure is present for this ssDNA sequence, shortening the effective contour length of the ssDNA. Our simulations were performed at the experimental temperature used by Nickels et al., 21°C, and a monovalent salt concentration of $[Na^+]$=5 M in order to mimic the high experimental $[Mg^{2+}]$ concentration. As the exFJC model calculations employed by Nickels et al.[17] assume fixed polymer endpoints, we also set out to explore the effect of origami compliance on the force in the structure by performing simulations on the 4.0 pN system using harmonic trap stiffnesses an order of magnitude larger and smaller than $k = 16.32\,\text{pN/nm}$. Finally, we performed additional simulations on the 4.0 pN system at $[Na^+]$=0.15 M, 0.5 M,

and 1.0 M to explore the effect of salt concentration on the results. In all cases, we simulated the strands both with secondary structure and without allowing secondary structure to form. Because transitions between HJ IsoI and IsoII conformations are very rare on the timescale of our simulations[2], we were unable to probe the effect of force on transition frequency. We therefore simulated each isomer separately and report results for both.

It is important to ensure that our simulations are sampling all relevant secondary structure, a potentially difficult task given both the possibility of the system becoming trapped in local minima for long stretches of simulation time and the large number of potential different secondary structures. To gauge whether we had sampled secondary structure sufficiently, we split our simulation output for each system in half and tracked which bases formed hydrogen bonds throughout the simulations (see Supporting Figures S3-S5). The hydrogen-bonding pattern looked similar enough between the two simulation halves to give us confidence that our secondary structure sampling is sufficient in the present case; see pages 8-11 of the Supporting Information for details. An additional consideration is oxDNA's inability to capture non-canonical base pairing, as mentioned in the *Introduction*. To explore this further, we ran our sequences through the Quadruplex forming G-Rich Sequences (QGRS) Mapper[79] to determine whether G quartets can form in our system. For the 162-nt and 228-nt designs, no G quartets are expected. For the 424-nt design, however, five G-quartet motifs (each with 2 stacked G tetrads) are theoretically possible. The consistency of the trends observed in our results across all three systems, detailed below, give us confidence that this limitation is not significant to our central results, however.

3.3.2 Results

The full results of our simulations are reported in Supporting Table S1. Figure 7 shows some representative one-sided forces crossing several interfaces along the ssDNA strand for

[2]Over $\sim 5 \times 10^{11}$ cumulative MD simulation steps ($\sim$7 ms), only 14 transitions were observed, and in each case, the HJ never reverted. This was reasonable given that the experimentally-observed transition times are on the order of tens of milliseconds.[17]

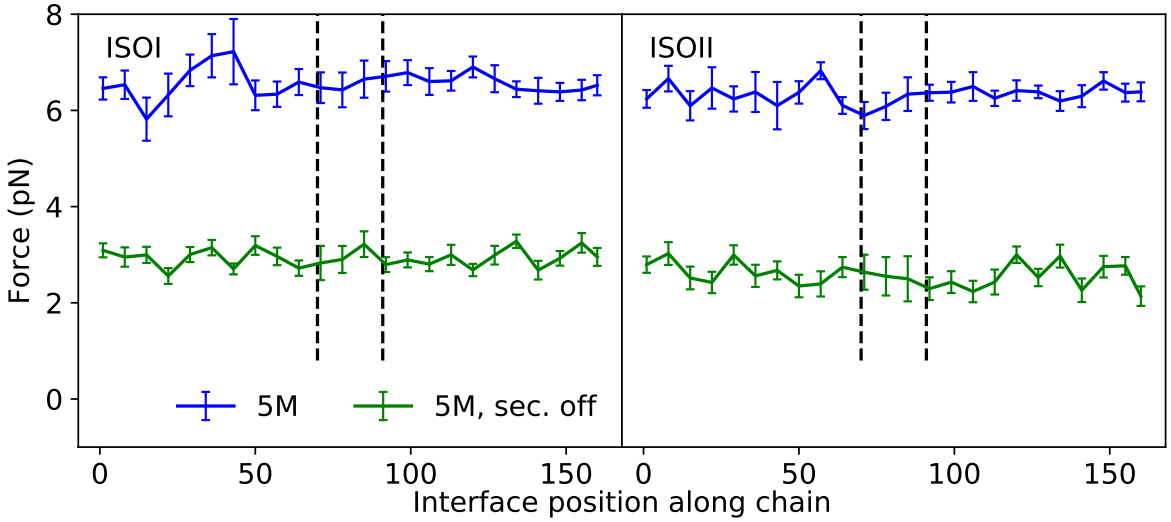

Figure 7: One-sided forces across interfaces at 24 different locations along the ssDNA strand for Nickels et al.[17]'s 4.0 pN design. The location of the HJ is denoted with black dashed lines. Simulations were performed at $[Na^+]$=5 M for IsoI (left) and IsoII (right), with secondary structure formation permitted (blue curves) and suppressed (green curves). Errors are standard deviations over 23 (left) or 24 (right) identical replica simulations of $\sim 10^9$ MD steps ($\sim$35 µs (left) and $\sim$47 µs (right) total simulation time).

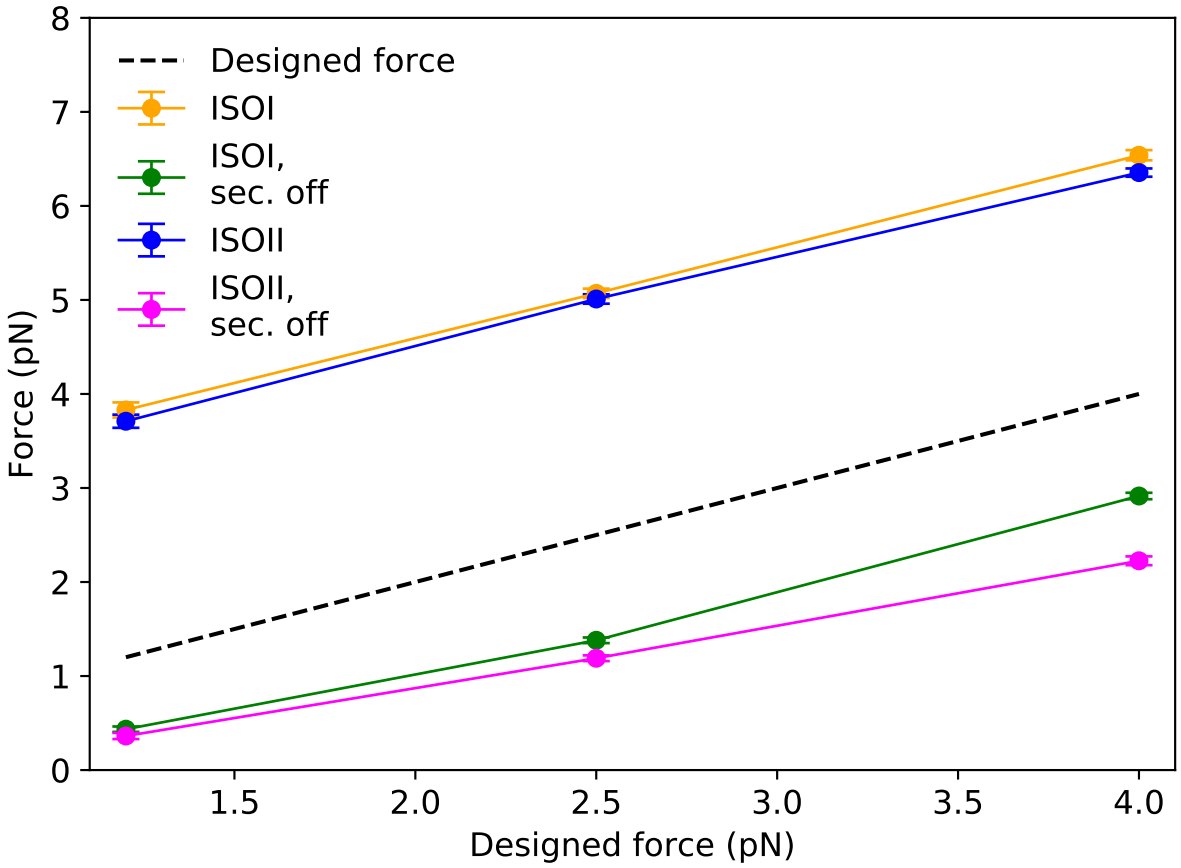

Figure 8: The force computed in simulations versus the 'designed' force. The latter is based on the exFJC model, using the parameters of Smith et al.[28]. 1:1 equivalence between the two is indicated by the dashed black line. In all cases, the measured force is larger than both the designed force (by about $\sim$2.5 pN) and the result when secondary structure is turned off (by about $\sim$3.6 pN). The force difference between IsoI and IsoII is always small.

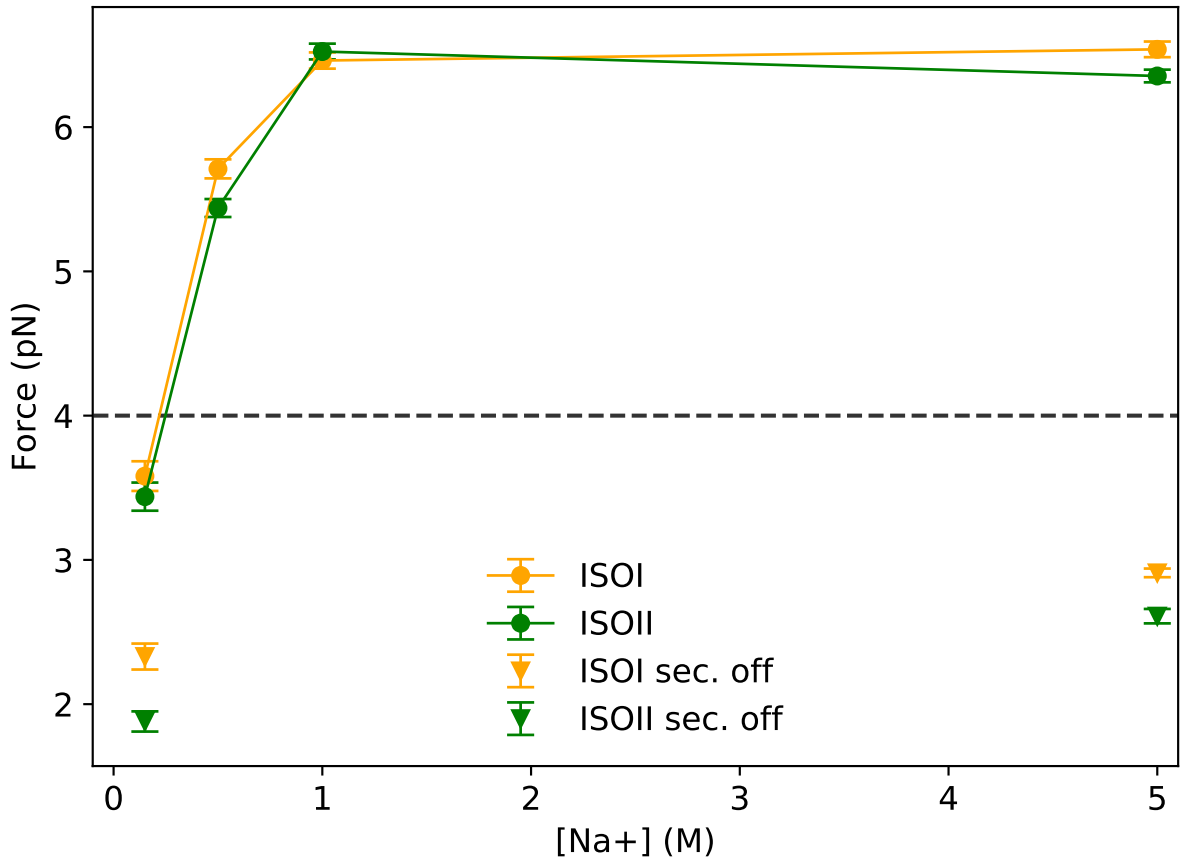

Figure 9: The effect of [Na^+] concentration on the measured force for the 4.0 pN design of Nickels et al.[17] (the black dashed line indicates the designed force and does not include any salt dependence). At low salt, electrostatic repulsion increasingly destabilizes secondary structure, leading to lower measured forces. This is corroborated by the comparatively smaller gap between low and high salt when secondary structure is not permitted to form.

the 4.0 pN design, where the interfaces are located immediately topologically upstream of the nucleotides indicated in the abscissa. Larger errors likely correlate with regions with an enhanced tendency to form secondary structure, because of the larger magnitude of the (positive and negative) forces across the interfaces in those regions; this effect was observed in Fig. 4. Only the projection of the force onto the direction of the trap separation is shown; forces along the orthogonal directions average to zero, as expected.

Figures 8-9 contain results for forces averaged over 24, 33, and 39 different interfaces distributed along the strand for the 4.0 pN 2.5 pN, and 1.2 pN designs, respectively; error bars represent the standard error of a weighted mean. Immediately evident in Fig. 8 is the substantial discrepancy between the forces as measured in simulation (blue and yellow curves) and both the Smith et al.[28] exFJC force predictions (black dashed line; ∼2.5 pN average discrepancy) and the forces in the absence of secondary structure (∼3.6 pN average discrepancy). Here, just as in the case of the simple 160-nt poly-T strand, forces in the absence of secondary structure are lower than the exFJC estimates; as aforementioned, this can be understood by considering that the fits performed by Smith et al.[28] averaged over secondary structure inherent to λ-phage ssDNA.

The presence of secondary structure obviously has a significant effect on internal force. In this case, however, another key driver of the disparity between exFJC predictions and forces measured in simulations may simply be the different salt concentrations under which the experiments of Smith et al.[28] and Nickels et al.[17] were carried out. The results of simulations of the 4.0 pN design performed at four different salt concentrations are shown in Figure 9. At $[Na^+]$=0.15M, which corresponds to the concentration at which Smith et al.[28] performed their exFJC fits, the average measured force is ∼3 pN lower than at the higher salt concentrations used by Nickels et al.[17], and much closer to the estimate of 4.0 pN obtained using Smith et al.[28]'s parameters. Caution is clearly needed when translating ssDNA elastic fit results performed under different conditions. When secondary structure is suppressed, the difference in force between the highest and lowest ionic strengths is only

$\sim$0.7 pN, underscoring secondary structure formation as the main driver of force variation with ion concentration. The remaining difference is attributable to the tendency of ssDNA to form more compact coils at higher salt concentration as increased screening reduces inter-phosphate repulsion.[71]

We also explored the effect of the compliance of the attachment points on internal ssDNA forces; see Figure S7 in the Supporting Information for full details. In summary, while decreasing the trap stiffness by an order of magnitude (from $\sim$16.32 pN/nm to $\sim$1.632 pN/nm) decreases the force by about 0.2 pN, increasing the stiffness by an order of magnitude has no discernible effect. As oxDNA has been elsewhere shown to reproduce the elastic properties of DNA origami well,[51,80] we can conclude that for these designs the assumption of Nickels et al.[17] that the origami is rigid does not affect the force estimate.

As a final note, we point out that the difference in force between the two HJ isomers is in all cases rather small: $\sim$0.1-0.5 pN, with the IsoI conformation leading to higher (or the same within error) forces than IsoII, as expected. Because the oxDNA model cannot fully capture the magnitude of the twist angle between the HJ arms,[53] however, we do not expect to perfectly reproduce the difference between the two isomers.

4 Conclusion

We have demonstrated a method for calculating the internal forces in ssDNA to high statistical precision ($\sim$0.05 pN). While systematic errors intrinsic to the oxDNA coarse-grained model can be expected to affect the absolute accuracy of our force calculations, oxDNA has elsewhere captured the mechanical behaviour of ssDNA and dsDNA well,[45,81,82] which gives us confidence that our predictions are much more realistic than those of simplified polymer model fits. Further, given the limited precision of experimental calibration methods ($\sim$2-5 pN[19,25]), we argue that oxDNA predictions supply a viable alternative – or at least complement – to these approaches. In addition to its utility in computing forces in ssDNA-

based force sensors, force clamp devices, and tensegrity nanostructures, our method can be expanded to calculate forces in more complex structures, such as DNA minicircles.[83,84] Furthermore, the method is general enough to be adapted to calculate forces in alternative coarse-grained models, including for non-DNA polymers like proteins.

A number of caveats should be kept in mind when interpreting our work. For one thing, we have assumed that origami structures were perfectly assembled, with no topologically incorrect strand routings and with all staples present. In experiments, defects which could compromise the effective stiffness of the origami or alter the length of the ssDNA spring are possible. Secondly, the parametrization of oxDNA was performed to capture the $[Na^+]$ dependence of secondary structure thermodynamics, so we relied on a mapping to an equivalent $[Na^+]$ in order to represent experiments that featured $[Mg^{2+}]$. This was not a problem for the current work, as experiments were carried out in a high-salt regime where the predicted force had reached its limiting value. For contexts involving lower $[Mg^{2+}]$, comparison of experiment and simulation may be less straightforward. Another consideration to bear in mind is the neglect of secondary structures involving non-canonical base pairs when calculating force averages. In systems where such motifs are expected to be relevant, deriving very accurate force estimates may necessitate the use of a coarse-grained model parameterized to treat non-Watson Crick base pairing. Lastly, it is possible that for high internal forces or low ionic strengths, the ssDNA tension may lead to non-elastic yielding events within origami designs. To capture such effects, the entire DNA origami structure would need to be simulated.

To obtain accurate estimates of internal force, precise experimental sequences must be simulated under relevant conditions. This is crucial because differences in secondary structure, salt concentration, stacking propensities, and stiffness of the endpoint traps can lead to errors in calculations that employ previously-obtained fit parameters with WLC and exFJC theoretical models, which also harbor fundamental deficiencies including neglect of excluded volume and base stacking. In particular, our results demonstrate that ignoring the difference

between the experimental ionic solution conditions and those at which fit parameters were derived is a significant driver of errors in ssDNA force estimates for the nanoscopic force clamp of Nickels et al.[17]. Future applications seeking to precisely determine internal forces of DNA, whether for the purposes of computationally modelling DNA elastic behavior[39,85] or for understanding biomechanical systems,[2] would benefit from the force estimates provided by oxDNA or similar coarse-grained models.

Acknowledgement

Portions of this manuscript appeared in an earlier form as part of MCE's doctoral thesis, which was published as part of the Springer Theses series.[86] MCE thanks the Rhodes Trust, the Natural Sciences and Engineering Research Council of Canada (NSERC), and Schmidt Science Fellows, in partnership with the Rhodes Trust, for financial support. We are grateful to the UK Materials and Molecular Modelling Hub for computational resources, which is partially funded by EPSRC (EP/P020194/1). Part of this work was performed using resources provided by the Cambridge Service for Data Driven Discovery (CSD3) operated by the University of Cambridge Research Computing Service (www.csd3.cam.ac.uk), provided by Dell EMC and Intel using Tier-2 funding from the Engineering and Physical Sciences Research Council (capital grant EP/P020259/1), and DiRAC funding from the Science and Technology Facilities Council (www.dirac.ac.uk). We are also grateful to Philipp Nickels and Tim Liedl for very helpful discussions.

Supporting Information Available

The following Supporting Information file is available free of charge, containing:

- full simulation details, including further information about the oxDNA thermostats and potentials;

- complete derivations for procedures outlined in the main text;
- details of the procedure to ensure adequate sampling over secondary structures;
- complete, tabulated simulation results; and
- additional figures highlighting simulated results.

References

(1) Alberts, B.; Johnson, A.; Lewis, J.; Raff, M.; Roberts, K.; Walter, P. *Molecular Biology of the Cell*, 5th ed.; Garland Science, 2008.

(2) Kramm, K.; Schröder, T.; Gouge, J.; Vera, A. M.; Gupta, K.; Heiss, F. B.; Liedl, T.; Engel, C.; Berger, I.; Vannini, A.; Tinnefeld, P.; Grohmann, D. DNA Origami-Based Single-Molecule Force Spectroscopy Elucidates RNA Polymerase III Pre-Initiation Complex Stability. *Nat Commun* **2020**, *11*, 2828.

(3) Uhler, C.; Shivashankar, G. V. Regulation of Genome Organization and Gene Expression by Nuclear Mechanotransduction. *Nat. Rev. Mol. Cell Biol.* **2017**, *18*, 717–727.

(4) Ingber, D. E. Cellular Mechanotransduction: Putting All the Pieces Together Again. *FASEB J.* **2006**, *20*, 811–827.

(5) Árnadóttir, J.; Chalfie, M. Eukaryotic Mechanosensitive Channels. *Annu. Rev. Biophys.* **2010**, *39*, 111–137.

(6) Wang, N. Review of Cellular Mechanotransduction. *J. Phys. D: Appl. Phys.* **2017**, *50*, 233002.

(7) Bustamante, C.; Chemla, Y. R.; Forde, N. R.; Izhaky, D. Mechanical Processes in Biochemistry. *Annu. Rev. Biochem.* **2004**, *73*, 705–748.

(8) Poh, Y.-C.; Chen, J.; Hong, Y.; Yi, H.; Zhang, S.; Chen, J.; Wu, D. C.; Wang, L.; Jia, Q.; Singh, R.; Yao, W.; Tan, Y.; Tajik, A.; Tanaka, T. S.; Wang, N. Generation of Organized Germ Layers from a Single Mouse Embryonic Stem Cell. *Nat. Commun.* **2014**, *5*, 4000.

(9) Kim, S. T.; Takeuchi, K.; Sun, Z.-Y. J.; Touma, M.; Castro, C. E.; Fahmy, A.; Lang, M. J.; Wagner, G.; Reinherz, E. L. The $\alpha\beta$ T Cell Receptor Is an Anisotropic Mechanosensor. *J. Biol. Chem.* **2009**, *284*, 31028–31037.

(10) Spillane, K. M.; Tolar, P. B Cell Antigen Extraction Is Regulated by Physical Properties of Antigen-Presenting Cells. *J. Cell Biol.* **2017**, *216*, 217–230.

(11) Levental, K. R.; Yu, H.; Kass, L.; Lakins, J. N.; Egeblad, M.; Erler, J. T.; Fong, S. F.; Csiszar, K.; Giaccia, A.; Weninger, W.; Yamauchi, M.; Gasser, D. L.; Weaver, V. M. Matrix Crosslinking Forces Tumor Progression by Enhancing Integrin Signaling. *Cell* **2009**, *139*, 891–906.

(12) Seeman, N. C. Nucleic Acid Junctions and Lattices. *J. Theor. Biol.* **1982**, *99*, 237–247.

(13) Seeman, N. C.; Sleiman, H. F. DNA Nanotechnology. *Nat. Rev. Mater.* **2018**, *3*, 17068.

(14) Gu, H.; Yang, W.; Seeman, N. C. DNA Scissors Device Used to Measure MutS Binding to DNA Mis-Pairs. *J. Am. Chem. Soc.* **2010**, *132*, 4352–4357.

(15) Cost, A.-L.; Ringer, P.; Chrostek-Grashoff, A.; Grashoff, C. How to Measure Molecular Forces in Cells: A Guide to Evaluating Genetically-Encoded FRET-Based Tension Sensors. *Cel. Mol. Bioeng.* **2015**, *8*, 96–105.

(16) Blanchard, A. T.; Salaita, K. Emerging Uses of DNA Mechanical Devices. *Science* **2019**, *365*, 1080–1081.

(17) Nickels, P. C.; Wunsch, B.; Holzmeister, P.; Bae, W.; Kneer, L. M.; Grohmann, D.;

Tinnefeld, P.; Liedl, T. Molecular Force Spectroscopy with a DNA Origami–Based Nanoscopic Force Clamp. *Science* **2016**, *354*, 305–307.

(18) Thubagere, A. J.; Li, W.; Johnson, R. F.; Chen, Z.; Doroudi, S.; Lee, Y. L.; Izatt, G.; Wittman, S.; Srinivas, N.; Woods, D.; Winfree, E.; Qian, L. A Cargo-Sorting DNA Robot. *Science* **2017**, *357*, eaan6558.

(19) Shroff, H.; Reinhard, B. M.; Siu, M.; Agarwal, H.; Spakowitz, A.; Liphardt, J. Biocompatible Force Sensor with Optical Readout and Dimensions of 6 Nm^3. *Nano Lett.* **2005**, *5*, 1509–1514.

(20) Brockman, J. M.; Blanchard, A. T.; Pui-Yan, V.; Derricotte, W. D.; Zhang, Y.; Fay, M. E.; Lam, W. A.; Evangelista, F. A.; Mattheyses, A. L.; Salaita, K. Mapping the 3D Orientation of Piconewton Integrin Traction Forces. *Nat. Methods* **2018**, *15*, 115–118.

(21) Funke, J. J.; Ketterer, P.; Lieleg, C.; Schunter, S.; Korber, P.; Dietz, H. Uncovering the Forces between Nucleosomes Using DNA Origami. *Sci. Adv.* **2016**, *2*, e1600974.

(22) Wang, X.; Ha, T. Defining Single Molecular Forces Required to Activate Integrin and Notch Signaling. *Science* **2013**, *340*, 991–994.

(23) Blakely, B. L.; Dumelin, C. E.; Trappmann, B.; McGregor, L. M.; Choi, C. K.; Anthony, P. C.; Duesterberg, V. K.; Baker, B. M.; Block, S. M.; Liu, D. R.; Chen, C. S. A DNA-Based Molecular Probe for Optically Reporting Cellular Traction Forces. *Nat. Methods* **2014**, *11*, 1229–1232.

(24) Zhang, Y.; Ge, C.; Zhu, C.; Salaita, K. DNA-Based Digital Tension Probes Reveal Integrin Forces during Early Cell Adhesion. *Nat. Commun.* **2014**, *5*, 5167.

(25) Dutta, P. K.; Zhang, Y.; Blanchard, A. T.; Ge, C.; Rushdi, M.; Weiss, K.; Zhu, C.;

Ke, Y.; Salaita, K. Programmable Multivalent DNA-Origami Tension Probes for Reporting Cellular Traction Forces. *Nano Lett.* **2018**, *18*, 4803–4811.

(26) Liu, Y.; Blanchfield, L.; Ma, V. P.-Y.; Andargachew, R.; Galior, K.; Liu, Z.; Evavold, B.; Salaita, K. DNA-Based Nanoparticle Tension Sensors Reveal That T-Cell Receptors Transmit Defined pN Forces to Their Antigens for Enhanced Fidelity. *Proc. Natl. Acad. Sci. U.S.A.* **2016**, *113*, 5610–5615.

(27) Ma, R.; Kellner, A. V.; Ma, V. P.-Y.; Su, H.; Deal, B. R.; Brockman, J. M.; Salaita, K. DNA Probes That Store Mechanical Information Reveal Transient Piconewton Forces Applied by T Cells. *Proc. Natl. Acad. Sci. U.S.A.* **2019**, *116*, 16949–16954.

(28) Smith, S. B.; Cui, Y.; Bustamante, C. Overstretching B-DNA: The Elastic Response of Individual Double-Stranded and Single-Stranded DNA Molecules. *Science* **1995**, *271*, 795–799.

(29) Camunas-Soler, J.; Ribezzi-Crivellari, M.; Ritort, F. Elastic Properties of Nucleic Acids by Single-Molecule Force Spectroscopy. *Annu. Rev. Biophys.* **2016**, *45*, 65–84.

(30) Zocchi, G. Controlling Proteins Through Molecular Springs. *Annu. Rev. Biophys.* **2009**, *38*, 75–88.

(31) Meng, F.; Sachs, F. Visualizing Dynamic Cytoplasmic Forces with a Compliance-Matched FRET Sensor. *J. Cell Sci.* **2011**, *124*, 261–269.

(32) Simmel, S. S.; Nickels, P. C.; Liedl, T. Wireframe and Tensegrity DNA Nanostructures. *Acc. Chem. Res.* **2014**, *47*, 1691–1699.

(33) Liedl, T.; Högberg, B.; Tytell, J.; Ingber, D. E.; Shih, W. M. Self-Assembly of Three-Dimensional Prestressed Tensegrity Structures from DNA. *Nat. Nanotechnol.* **2010**, *5*, 520–524.

(34) Goodman, R. P.; Schaap, I. A. T.; Tardin, C. F.; Erben, C. M.; Berry, R. M.; Schmidt, C. F.; Turberfield, A. J. Rapid Chiral Assembly of Rigid DNA Building Blocks for Molecular Nanofabrication. *Science* **2005**, *310*, 1661–1665.

(35) He, Y.; Ye, T.; Su, M.; Zhang, C.; Ribbe, A. E.; Jiang, W.; Mao, C. Hierarchical Self-Assembly of DNA into Symmetric Supramolecular Polyhedra. *Nature* **2008**, *452*, 198–201.

(36) Marras, A. E.; Zhou, L.; Su, H.-J.; Castro, C. E. Programmable Motion of DNA Origami Mechanisms. *Proc. Natl. Acad. Sci. U.S.A.* **2015**, *112*, 713–718.

(37) Douglas, S. M.; Bachelet, I.; Church, G. M. A Logic-Gated Nanorobot for Targeted Transport of Molecular Payloads. *Science* **2012**, *335*, 831–834.

(38) Lo, P. K.; Karam, P.; Aldaye, F. A.; McLaughlin, C. K.; Hamblin, G. D.; Cosa, G.; Sleiman, H. F. Loading and Selective Release of Cargo in DNA Nanotubes with Longitudinal Variation. *Nat. Chem.* **2010**, *2*, 319–328.

(39) Kim, D.-N.; Kilchherr, F.; Dietz, H.; Bathe, M. Quantitative Prediction of 3D Solution Shape and Flexibility of Nucleic Acid Nanostructures. *Nucleic Acids Res.* **2012**, *40*, 2862–2868.

(40) Reshetnikov, R. V.; Stolyarova, A. V.; Zalevsky, A. O.; Panteleev, D. Y.; Pavlova, G. V.; Klinov, D. V.; Golovin, A. V.; Protopopova, A. D. A Coarse-Grained Model for DNA Origami. *Nucleic Acids Res.* **2018**, *46*, 1102–1112.

(41) Evans, E.; Ritchie, K. Dynamic Strength of Molecular Adhesion Bonds. *Biophys. J.* **1997**, *72*, 1541–1555.

(42) Bullerjahn, J. T.; Sturm, S.; Kroy, K. Theory of Rapid Force Spectroscopy. *Nat. Commun.* **2014**, *5*, 4463.

(43) Odijk, T. Stiff Chains and Filaments under Tension. *Macromolecules* **1995**, *28*, 7016–7018.

(44) Rubinstein, M.; Colby, R. *Polymer Physics*; Oxford University Press, 2003.

(45) Ouldridge, T. E.; Louis, A. A.; Doye, J. P. K. Structural, Mechanical, and Thermodynamic Properties of a Coarse-Grained DNA Model. *J. Chem. Phys.* **2011**, *134*, 085101.

(46) Šulc, P.; Romano, F.; Ouldridge, T. E.; Rovigatti, L.; Doye, J. P. K.; Louis, A. A. Sequence-Dependent Thermodynamics of a Coarse-Grained DNA Model. *J. Chem. Phys.* **2012**, *137*, 135101.

(47) Snodin, B. E. K.; Randisi, F.; Mosayebi, M.; Šulc, P.; Schreck, J. S.; Romano, F.; Ouldridge, T. E.; Tsukanov, R.; Nir, E.; Louis, A. A.; Doye, J. P. K. Introducing Improved Structural Properties and Salt Dependence into a Coarse-Grained Model of DNA. *J. Chem. Phys.* **2015**, *142*, 234901.

(48) Matek, C.; Šulc, P.; Randisi, F.; Doye, J. P. K.; Louis, A. A. Coarse-Grained Modelling of Supercoiled RNA. *J. Chem. Phys.* **2015**, *143*, 243122.

(49) Skoruppa, E.; Nomidis, S. K.; Marko, J. F.; Carlon, E. Bend-Induced Twist Waves and the Structure of Nucleosomal DNA. *Phys. Rev. Lett.* **2018**, *121*, 088101.

(50) Romano, F.; Chakraborty, D.; Doye, J. P. K.; Ouldridge, T. E.; Louis, A. A. Coarse-Grained Simulations of DNA Overstretching. *J. Chem. Phys.* **2013**, *138*, 085101.

(51) Sharma, R.; Schreck, J. S.; Romano, F.; Louis, A. A.; Doye, J. P. K. Characterizing the Motion of Jointed DNA Nanostructures Using a Coarse-Grained Model. *ACS Nano* **2017**, *11*, 12426–12435.

(52) Shi, Z.; Castro, C. E.; Arya, G. Conformational Dynamics of Mechanically Compliant DNA Nanostructures from Coarse-Grained Molecular Dynamics Simulations. *ACS Nano* **2017**, *11*, 4617–4630.

(53) Snodin, B. E. K.; Schreck, J. S.; Romano, F.; Louis, A. A.; Doye, J. P. K. Coarse-Grained Modelling of the Structural Properties of DNA Origami. *Nucleic Acids Res.* **2019**, *47*, 1585–1597.

(54) Engel, M. C.; Smith, D. M.; Jobst, M. A.; Sajfutdinow, M.; Liedl, T.; Romano, F.; Rovigatti, L.; Louis, A. A.; Doye, J. P. K. Force-Induced Unravelling of DNA Origami. *ACS Nano* **2018**, *12*, 6734–6747.

(55) Schreck, J. S.; Ouldridge, T. E.; Romano, F.; Šulc, P.; Shaw, L. P.; Louis, A. A.; Doye, J. P. DNA Hairpins Destabilize Duplexes Primarily by Promoting Melting Rather than by Inhibiting Hybridization. *Nucleic Acids Res.* **2015**, *43*, 6181–6190.

(56) Andersen, H. C. Molecular Dynamics Simulations at Constant Pressure and/or Temperature. *J. Chem. Phys.* **1980**, *72*, 2384–2393.

(57) Russo, J.; Tartaglia, P.; Sciortino, F. Reversible Gels of Patchy Particles: Role of the Valence. *J. Chem. Phys.* **2009**, *131*, 014504.

(58) Sulc, P. Coarse-Grained Modelling of Nucleic Acids. Ph.D. thesis, Oxford University, UK, 2014.

(59) Frenkel, D.; Smit, B. In *Understanding Molecular Simulation (Second Edition)*, second edition ed.; Frenkel, D., Smit, B., Eds.; Academic Press: San Diego, 2002; pp 139–163.

(60) Padding, J. T.; Louis, A. A. Hydrodynamic Interactions and Brownian Forces in Colloidal Suspensions: Coarse-Graining over Time and Length Scales. *Phys. Rev. E* **2006**, *74*, 031402.

(61) Snodin, B. E. K.; Romano, F.; Rovigatti, L.; Ouldridge, T. E.; Louis, A. A.; Doye, J. P. K. Direct Simulation of the Self-Assembly of a Small DNA Origami. *ACS Nano* **2016**, *10*, 1724–1737.

(62) Chen, P.; Li, C. M. Nanopore Unstacking of Single-Stranded DNA Helices. *Small* **2007**, *3*, 1204–1208.

(63) Calladine, C. R., Ed. *Understanding DNA the Molecule & How It Works.*, 3rd ed.; Elsevier Academic Press: Amsterdam ;, 2004.

(64) Woodside, M. T.; Block, S. M. Reconstructing Folding Energy Landscapes by Single-Molecule Force Spectroscopy. *Annu. Rev. Biophys.* **2014**, *43*, 19–39.

(65) Hohng, S.; Zhou, R.; Nahas, M. K.; Yu, J.; Schulten, K.; Lilley, D. M. J.; Ha, T. Fluorescence-Force Spectroscopy Maps Two-Dimensional Reaction Landscape of the Holliday Junction. *Science* **2007**, *318*, 279–283.

(66) Marko, J. F.; Siggia, E. D. Stretching DNA. *Macromolecules* **1995**, *28*, 8759–877–.

(67) Gross, P.; Laurens, N.; Oddershede, L. B.; Bockelmann, U.; Peterman, E. J. G.; Wuite, G. J. L. Quantifying How DNA Stretches, Melts and Changes Twist under Tension. *Nat. Phys.* **2011**, *7*, 731–736.

(68) Nomidis, S. K.; Kriegel, F.; Vanderlinden, W.; Lipfert, J.; Carlon, E. Twist-Bend Coupling and the Torsional Response of Double-Stranded DNA. *Phys. Rev. Lett.* **2017**, *118*, 217801.

(69) Huguet, J. M.; Bizarro, C. V.; Forns, N.; Smith, S. B.; Bustamante, C.; Ritort, F. Single-Molecule Derivation of Salt Dependent Base-Pair Free Energies in DNA. *Proc. Natl. Acad. Sci. U.S.A.* **2010**, *107*, 15431–15436.

(70) Bosco, A.; Camunas-Soler, J.; Ritort, F. Elastic Properties and Secondary Structure Formation of Single-Stranded DNA at Monovalent and Divalent Salt Conditions. *Nucleic Acids Res.* **2014**, *42*, 2064–2074.

(71) McIntosh, D. B.; Duggan, G.; Gouil, Q.; Saleh, O. A. Sequence-Dependent Elasticity

and Electrostatics of Single-Stranded DNA: Signatures of Base-Stacking. *Biophys. J.* **2014**, *106*, 659–666.

(72) Laurence, T. A.; Kong, X.; Jager, M.; Weiss, S. Probing Structural Heterogeneities and Fluctuations of Nucleic Acids and Denatured Proteins. *Proc. Natl. Acad. Sci. U.S.A.* **2005**, *102*, 17348–17353.

(73) Jacobson, D. R.; McIntosh, D. B.; Stevens, M. J.; Rubinstein, M.; Saleh, O. A. Single-Stranded Nucleic Acid Elasticity Arises from Internal Electrostatic Tension. *Proc. Natl. Acad. Sci. U.S.A.* **2017**, *114*, 5095–5100.

(74) Lei, D.; Marras, A. E.; Liu, J.; Huang, C.-M.; Zhou, L.; Castro, C. E.; Su, H.-J.; Ren, G. Three-Dimensional Structural Dynamics of DNA Origami Bennett Linkages Using Individual-Particle Electron Tomography. *Nat. Commun.* **2018**, *9*, 592.

(75) Kauert, D. J.; Kurth, T.; Liedl, T.; Seidel, R. Direct Mechanical Measurements Reveal the Material Properties of Three-Dimensional DNA Origami. *Nano Lett.* **2011**, *11*, 5558–5563.

(76) Pfitzner, E.; Wachauf, C.; Kilchherr, F.; Pelz, B.; Shih, W. M.; Rief, M.; Dietz, H. Rigid DNA Beams for High-Resolution Single-Molecule Mechanics. *Angew. Chem. Int. Ed.* **2013**, *52*, 7766–7771.

(77) Murphy, M.; Rasnik, I.; Cheng, W.; Lohman, T. M.; Ha, T. Probing Single-Stranded DNA Conformational Flexibility Using Fluorescence Spectroscopy. *Biophys. J.* **2004**, *86*, 2530–2537.

(78) Martin, T. G.; Dietz, H. Magnesium-Free Self-Assembly of Multi-Layer DNA Objects. *Nat. Commun.* **2012**, *3*, 1103.

(79) Kikin, O.; D'Antonio, L.; Bagga, P. S. QGRS Mapper: A Web-Based Server for Pre-

dicting G-Quadruplexes in Nucleotide Sequences. *Nucleic Acids Res.* **2006**, *34*, W676–W682.

(80) Tortora, M. M. C.; Mishra, G.; Presern, D.; Doye, J. P. K. Chiral Shape Fluctuations and the Origin of Chirality in Cholesteric Phases of DNA Origamis. *Sci. Adv.* **2020**, *6*, eaaw8331.

(81) Mosayebi, M.; Louis, A. A.; Doye, J. P. K.; Ouldridge, T. E. Force-Induced Rupture of a DNA Duplex: From Fundamentals to Force Sensors. *ACS Nano* **2015**, *9*, 11993–12003.

(82) Nomidis, S. K.; Skoruppa, E.; Carlon, E.; Marko, J. F. Twist-Bend Coupling and the Statistical Mechanics of the Twistable Wormlike-Chain Model of DNA: Perturbation Theory and Beyond. *Phys. Rev. E* **2019**, *99*, 032414.

(83) Sutthibutpong, T.; Matek, C.; Benham, C.; Slade, G. G.; Noy, A.; Laughton, C.; Doye, J. P. K.; Louis, A. A.; Harris, S. A. Long-Range Correlations in the Mechanics of Small DNA Circles under Topological Stress Revealed by Multi-Scale Simulation. *Nucleic Acids Res.* **2016**, 9121–9130.

(84) Joffroy, B.; Uca, Y. O.; Prešern, D.; Doye, J. P. K.; Schmidt, T. L. Rolling Circle Amplification Shows a Sinusoidal Template Length-Dependent Amplification Bias. *Nucleic Acids Res.* **2018**, *46*, 538–545.

(85) Castro, C. E.; Kilchherr, F.; Kim, D.-N.; Shiao, E. L.; Wauer, T.; Wortmann, P.; Bathe, M.; Dietz, H. A Primer to Scaffolded DNA Origami. *Nat. Methods* **2011**, *8*, 221–229.

(86) Engel, M. *DNA Systems Under Internal and External Forcing: An Exploration Using Coarse-Grained Modelling*; Springer International Publishing, 2019.

Graphical TOC Entry